Geochimica et Cosmochimica Acta, Vol. 69, No. 13, pp. 3321–3335, 2005

0016-7037/05 $30.00 + .00

doi:10.1016/j.gca.2005.01.028

Gold partitioning in melt-vapor-brine systems

Adam C. Simon,[1,*,†] Mark R. Frank,[2] Thomas Pettke,[3] Philip A. Candela,[1] Philip M. Piccoli,[1] and Christoph A. Heinrich[3]

[1]Laboratory for Mineral Deposits Research, Department of Geology, University of Maryland, College Park, Maryland 20742, USA
[2]Department of Geology and Environmental Geosciences, Davis Hall 312, Normal Road, Northern Illinois University, DeKalb, Illinois 60115, USA
[3]Isotope Geochemistry and Mineral Resources, Federal Institute of Technology, ETH Zentrum NO, CH-8092, Zurich, Switzerland

(*Received June* 14, 2004; *accepted in revised form January* 28, 2005)

Abstract—We used laser-ablation inductively coupled plasma mass spectrometry to measure the solubility of gold in synthetic sulfur-free vapor and brine fluid inclusions in a vapor + brine + haplogranite + magnetite + gold metal assemblage. Experiments were conducted at 800°C, oxygen fugacity buffered at Ni-NiO (NNO), and pressures ranging from 110 to 145 MPa. The wt% NaCl eq. of vapor increases from 2.3 to 19 and that of brine decreases from 57 to 35 with increasing pressure. The composition of the vapors and brines are dominated by NaCl + KCl + $FeCl_2$ + H_2O. Gold concentrations in vapor and brine decrease from 36 to 5 and 50 to 28 μg/g, respectively, and the calculated vapor:brine partition coefficients for gold decrease from 0.72 to 0.17 as pressure decreases from 145 to 110 MPa. These data are consistent with the thermodynamic boundary condition that the concentration of gold in the vapor and brine must approach a common value as the critical pressure is approached along the 800°C isotherm in the NaCl-KCl-$FeCl_2$-HCl-H_2O system.

We use the equilibrium constant for gold dissolution as $AuOH^0$, extrapolated from lower temperature and overlapping pressure range, to calculate expected concentrations of $AuOH^0$ in our experimental vapors. These calculations suggest that a significant quantity of gold in our experimental vapors is present as a non-hydroxide species. Possible chloridogold(I) species are hypothesized based on the positively correlated gold and chloride concentrations in our experimental vapors. The absolute concentration of gold in our synthetic vapor, brine, and melt and calculated mass partition coefficients for gold between these physicochemically distinct magmatic phases suggests that gold solubility in aqueous fluids is a function of aqueous phase salinity, specifically total chloride concentration, at magmatic conditions. However, though we highlight here the effect of salinity, the combination of our data with data sets from lower temperatures evinces a significant decrease in gold solubility as temperature drops from 800°C to 600°C. This decrease in solubility has implications for gold deposition from ascending magmatic fluids. *Copyright © 2005 Elsevier Ltd*

1. INTRODUCTION

A variety of structural, fluid inclusion, isotopic, and experimental evidence suggests that aqueous fluids evolved from mid- to upper-crustal magma bodies are the primary gold-transporting agents responsible for the formation of gold-rich porphyry-type ore deposits (Emmons, 1927; Sillitoe, 1979, 1989, 1993, 2000; Burnham, 1979; Titley, 1981; Singer and Cox, 1986; Richards et al., 1991; Vila and Sillitoe, 1991; Hedenquist and Lowenstern, 1994; Lang et al., 1995; Shinohara and Kazahaya, 1995; Thompson et al., 1995; Gammons and Williams-Jones, 1997; Shinohara and Hedenquist, 1997; Hedenquist et al., 1998; Ulrich et al., 2001; Ulrich et al., 2001; Marschik and Fontboté, 2001; Frank et al., 2002; Halter et al., 2002; Candela, 2003; Requia et al., 2003). The gold-bearing fluid is hypothesized to have exsolved from the melt phase as the latter becomes volatile-phase-saturated owing to decompression and/or crystallization of anhydrous mineral phases (Burnham, 1979). A limited number of experimental investigations (Candela and Holland, 1984; Williams et al., 1995; Frank et al., 2002; Simon et al., 2004) and studies of natural systems (Audétat et al., 2000; Audétat and Pettke, 2003) have demonstrated that ore metals such as copper, gold, and iron partition strongly into an exsolved aqueous phase at near-magmatic conditions. The aqueous phase, once exsolved from the melt, can scavenge ore metals from the melt and, owing to its lower density relative to the surrounding melt ± crystals, ascend through the melt column and deposit its solute load in response to changes in pressure, temperature, acidity, salinity, oxygen, and sulfur fugacities, inter alia (Henley and McNabb, 1978).

Although there is general agreement that melts supply gold to an exsolved aqueous fluid phase (Hedenquist and Lowenstern, 1994; Bodnar, 1995), the story is complicated by the fact that melts can saturate with and exsolve more than one physicochemically distinct aqueous phase. Fluid inclusion data from natural ore-bearing magmatic systems indicate that melts undergoing volatile exsolution at subcritical conditions commonly exsolve magmatic volatile phases that can be approximated by the NaCl-H_2O binary system (Roedder, 1984; Bodnar et al., 1985). Examination of the pressure-volume-temperature-composition (*PVTX*) phase relations in the NaCl-H_2O system (Fig. 1) indicates that a water-chloride fluid may commonly separate into coexisting low-salinity aqueous vapor and hypersaline liquid (i.e., brine) at the prevailing range of *PT* conditions associated with magmatic intrusions in Earth's upper crust (Sourirajan and Kennedy, 1962; Henley and McNabb, 1978; Roedder, 1984; Bodnar et al., 1985; Chou, 1987a; Fournier, 1987). Both the vapor phase and the brine phase scavenge gold from the melt phase, so there is significant

* Author to whom correspondence should be addressed (asimon@jhu.edu).
† *Present address:* Department of Earth and Planetary Sciences, Johns Hopkins University, Baltimore, MD 21218, USA.

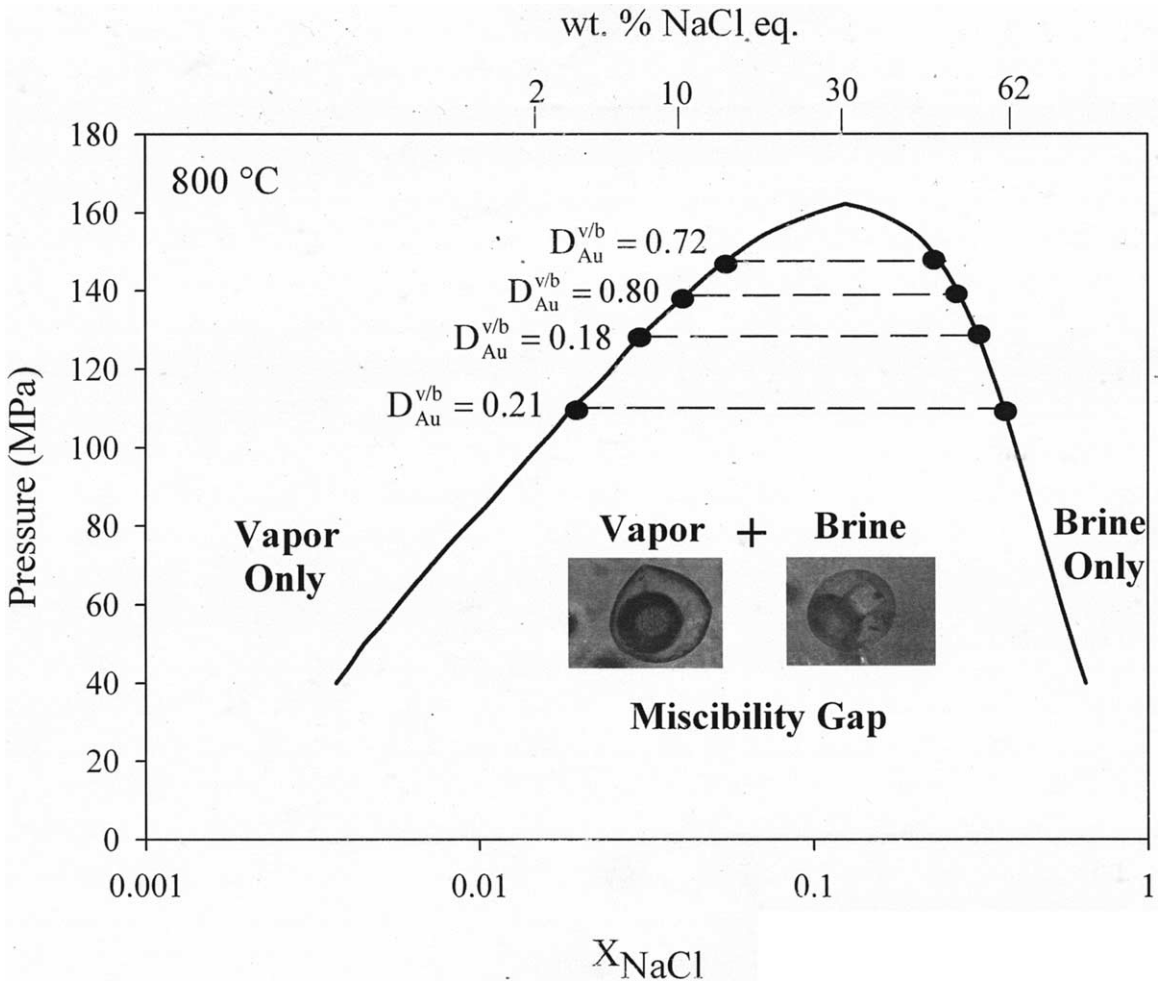

Fig. 1. Isothermal section of the system NaCl-H_2O at 800°C (modeled after Anderko and Pitzer, 1993). X_{NaCl} = mole fraction of NaCl in the pure NaCl-H_2O system. The curve outlines the miscibility gap as a function of pressure at 800°C; within this gap, vapor and brine coexist as two immiscible and physicochemically distinct fluids. Partition coefficients for gold were calculated from LA-ICPMS absolute gold concentrations determined by analyzing synthetic coexisting experimental vapor and brine fluid inclusions produced in our study. The inset photomicrographs of vapor (liquid + vapor bubble at ambient conditions) and brine (liquid + vapor bubble + halite ± other daughter crystals at ambient conditions) are from an experiment at 140 MPa and 800°C. Salinity expressed in units of wt% NaCl eq. values are presented along the upper abscissa; note that the upper abscissa is not a linear scale.

interest in quantifying the relative gold-scavenging capability of these two physicochemically distinct magmatic fluids. There is a growing body of data supporting a role in metal transport for CO_2-bearing volatile phases (Lowenstern, 2001); the current study focuses on CO_2-free Au-saturated NaCl-KCl-$FeCl_2$-HCl-H_2O fluids.

Recent studies employing laser-ablation inductively coupled plasma mass spectrometry (LA-ICPMS) to quantify the solute load of individual natural fluid inclusions from ore-bearing systems have yielded data which suggest a lack of consistency in the relative ability of magmatic vapor and brine to scavenge and transport gold in magmatic-hydrothermal environments. Heinrich et al. (1999) and Ulrich et al. (1999) report gold concentrations of natural vapor and brine fluid inclusions from the gold-rich porphyry-type ore deposit at Grasberg, Indonesia, that yield a calculated partition coefficient for gold between vapor and brine of $D_{Au}^{v/b} \approx 39$. Heinrich et al. (1999) cite the preferential partitioning of sulfur into vapor relative to brine (Drummond and Ohmoto, 1985) and postulate the existence of a gold-bisulfide complex to explain the preferential partitioning of gold into the vapor phase. Ulrich et al. (1999) also report gold concentrations of natural coexisting vapor and brine fluid inclusions from Bajo de la Alumbrera, Argentina, that yield a calculated partition coefficient of $D_{Au}^{v/b} \approx 0.7$ To date, there are no experimental data that allow us explain the inverse nature of the partition coefficient for gold in these two ore deposits that formed at similar *PVTX* conditions.

In an attempt to elucidate the effect of sulfur on gold partitioning into a fluid, Loucks and Mavrogenes (1999) determined gold solubility in pyrite-saturated supercritical hypersaline aqueous solutions at 550°C–725°C and 110–400 MPa. These authors report data suggesting that gold may be transported as a gold-sulfide species and, furthermore, that gold-chloride complexes are unimportant in transporting gold at all geologically

Table 1. Starting composition of synthetic haplogranite. Chemical composition of the starting glass used in all experiments as determined by XRF (Frank, 2001). LOI = loss on ignition.

Oxide	wt%
SiO_2	75.18
Al_2O_3	11.09
K_2O	4.43
Na_2O	3.67
CaO	0.17
Fe_2O_3	0.04
MnO	0.01
MgO	0.10
TiO_2	0.03
P_2O_5	0.03
LOI	4.51
Total	99.26

relevant pH and redox conditions. These data appear to confirm the existence of a gold-bisulfide complex in aqueous solutions at the *PT* conditions attending the evolution of magmatic-hydrothermal environments; however, it should be noted that Loucks and Mavrogenes (1999) aimed to evaluate gold solubility in aqueous fluids in equilibrium with mineral pH buffers. Several studies demonstrate that the acidity of magmatic fluids during the transport of ore metals can be significantly higher than the acidity at the time of the neutralization process (Williams et al., 1997; Piccoli et al., 1999; Frank et al., 1998). In a separate attempt to evaluate the role of sulfur on the partitioning behavior of gold, Frank (2001) reports experiments at 800°C, 100 MPa, and oxygen fugacity buffered at the nickel + nickel-oxide solid state oxygen fugacity buffer ($f_{O_2} = NNO$) in a vapor + brine + haplogranite melt + intermediate solid solution + gold metal assemblage. Intermediate solid solution (*iss*) is a sulfur-deficient phase with the stoichiometry $CuFeS_{2-x}$. Frank (2001) quantified the gold content of synthetic vapor and brine fluid inclusions, trapped in quartz microfractures, using LA-ICPMS and reported that $D_{Au}^{vb} < 1$. These studies, involving the analysis of both natural and synthetic magmatic fluids, have demonstrated that the partitioning behavior of gold in a vapor- + brine-saturated assemblage at near-magmatic conditions attending the evolution of ore-forming magmatic-hydrothermal systems remains ambiguous.

Here we report the first experimental data, to our knowledge, at magmatic conditions that elucidate the partitioning behavior of gold in a sulfur-free, vapor + brine + haplogranite + gold metal assemblage, as a first step to quantifying the variable vapor-brine partitioning behavior of gold across a range of *PTX* conditions applicable to the development of natural magmatic-hydrothermal environments. The data presented here elucidate specifically the effects of pressure and chlorinity on the relative abilities of magmatic vapor and brine to scavenge and transport gold within the magmatic-hydrothermal environment.

2. PROCEDURES

2.1. Experimental Design

We performed experiments that allow us to trap coexisting vapor and brine as fluid inclusions in prefractured quartz chips at the *PVTX* run conditions. The runs were well constrained with respect to temperature, pressure, and fluid-phase acidity and oxygen fugacity. Whereas the experiments were designed to lie within the brine-undersaturated vapor-only field of the model NaCl-H_2O system, all runs were vapor plus brine saturated as explained below. Experiments were conducted at 800°C, $f_{O_2} = NNO$, and pressures of 110, 130, 140, and 145 MPa. The experimental pressure range corresponds to lithostatic pressures in Earth's crust between ~4 and ~6 km; it is within the pressure range where the magmatic fluids that ultimately yield gold-rich porphyry-type ore deposits are thought to exsolve from gold-bearing felsic melts (Henley and McNabb, 1978; Burnham, 1979; Sillitoe, 2000). Experiments were performed at 800°C to expedite equilibration between all phase components in the experimental charge and to prevent the crystallization of silicate and/or oxide phases during the experiments which could produce compositional heterogeneities in the melt. The bulk salinity of starting aqueous fluids was set to lie in the vapor-only field just outside the 800°C vapor-brine solvus of the model NaCl-H_2O system (Bodnar et al., 1985) at all pressures in a magnetite–haplogranite melt–vapor–gold metal capsule assemblage. However, fluid inclusions trapped in prefractured quartz preserve both vapor and brine, indicating that our experiments were within the two-phase vapor + brine miscibility gap in the more complex NaCl-KCl-$FeCl_2$-HCl-H_2O system. The mass proportion of vapor to brine in all experiments is >95:1, as determined by using the lever rule and the salinities of the initial aqueous solution and measured wt% NaCl eq. values for the vapor and brine fluid inclusions.

2.2. Starting Materials

The starting synthetic haplogranite glass has the composition of a 100 MPa minimum melt, $Qz_{0.38}Ab_{0.33}$ $Or_{0.29}$ on an anhydrous basis, with a solidus temperature of ~710°C. The starting chemical composition of the haplogranite glass was determined by x-ray fluorescence (XRF) and is provided in Table 1. Starting aqueous solutions were prepared with reagent grade NaCl and KCl and aqueous HCl. The molarity of HCl (11.6 M) in the reagent was determined by titration. The molar ratio of Na:K:H was set to unity in all starting aqueous solutions. The chemical composition of the starting fluids is provided in Table 2. The reported uncertainty in fluid chemistry reflects estimated errors in the measured mass (NaCl and KCl) and volume (HCl), based on multiple measurements. Magnetite was included in all charges to ensure that the experimental fluids were magnetite saturated to more closely approximate natural magmatic fluids containing iron as a major

Table 2. Composition of starting aqueous solutions. The initial wt% NaCl eq. values were chosen from the data of Bodnar et al. (1985). The masses of NaCl and KCl and volume of HCl added to each starting aqueous mix were calculated from the wt% NaCl eq. values by imposing the criterion that the molar ratio of Na:K and Na:H equals one.

P (MPa)	Number of Runs	Initial wt% NaCl eq.	NaCl μg/g (±2σ)	KCl μg/g (±2σ)	HCl μg/mL (±2σ)
110	3	2.5	10000 ± 210	12700 ± 255	6200 ± 125
130	4	5	18331 ± 366	23300 ± 465	11400 ± 230
140	2	10	33300 ± 660	42500 ± 850	20700 ± 410
145	3	20	66000 ± 1300	85000 ± 1700	41000 ± 825

solute (Heinrich et al., 1992; Simon et al., 2004). Electron probe microanalysis (EPMA) data indicate that magnetite was nearly end-member Fe_3O_4 ($a^{mt}_{Fe_3O_4} \approx 1$). A haplogranite melt was included because we aimed to investigate potential melt-vapor-brine exchange relationships between iron, sodium, and potassium as well as elucidate the behavior of gold in a melt-magnetite-vapor-brine assemblage. The starting magnetite:melt:fluid mass ratio was 1:1:2.5 in all experiments. Prefractured quartz chips were prepared from inclusion-free and optically-clear quartz from Minas Gerais, Brazil (obtained from the Harvard Mineral Museum). Chips of quartz were cut to dimensions of ~3 mm width by ~1.5 cm length. The chips were heated to 350°C and held at that temperature for 30 minutes. The chips were then dumped into a room-temperature bath of doubly deionized distilled water. This sudden and dramatic temperature change produces a pervasive fracture network throughout the chip. Chips were then dried at 110°C for 24 hours to remove water.

2.3. Experimental Details

Gold capsules (4.8 mm ID, 5 mm OD, 30 mm length) were loaded with 40 mg magnetite (Cornwall, Pennsylvania), 40 mg synthetic haplogranite glass, a prefractured quartz chip, and 100 μL of starting aqueous solution. The loaded capsules were immersed in dry ice and welded shut. Sealed capsules were placed in a drying oven (110°C) for 4 hours, and maintenance of capsule mass (±3 mg) was used to verify the integrity of welded capsules. The capsules were placed inside cold-seal René-41 pressure vessels and pressurized with water. The vessels were heated inside doubly wound tube furnaces. Charges were pressurized to 50 MPa, heated to 800°C, and then pressurized to the final run pressure. Temperatures were measured with type K (Chromel-Alumel) external thermocouples that were calibrated against internal thermocouples in the presence of the water-pressure medium for each experimental vessel. The temperature gradient in each experimental vessel was minimized by maintaining the hot end of the vessel and the furnace at a 10° angle from horizontal (following Charles and Vidale, 1982). The maximum temperature gradient at all pressures was ± 5°C over the 3 cm long capsule, as determined by internal calibration in the presence of the water-pressure medium. The combination of a low temperature gradient and tilted vessel position minimizes the potential for thermally induced convection gradients, and this in turn retards premature healing of the prefractured quartz chips (Simon et al., 2003a). This lack of premature healing is critical to the experimental goal of trapping aqueous fluids that have equilibrated with all the phase components of the charge.

Pressure was imposed by an air-driven water-pressure intensifier and monitored with Bourdon-tube gauges (±2 MPa) calibrated against a factory-calibrated Heise gauge. The use of René-41 vessels, composed of a Ni-based alloy, coupled with the thermal dissociation of the water pressure medium ($2H_2O = 2H_2 + O_2$) and the ensuing establishment within 24 hours (Chou, 1987b) of osmotic equilibrium between the charge and the pressure buffer imposes a hydrogen fugacity equal to the nickel–nickel oxide (NNO) solid-state oxygen fugacity buffer on the experimental charge. At 800°C and 100 MPa, the experimental vessels used in this study have oxygen fugacities of $\log f_{O_2} = -14.0 \pm 0.1$, as determined in our laboratory using the Ag-AgCl sensor technique (Frank, 2001). Experiments were quenched isobarically along a two-stage cooling path involving air-stream cooling from 800°C to 200°C over a period of two minutes followed by immersion in an ambient-temperature water bath. Three reconnaissance experiments were performed in rapid-quench vessels (quench time is on the order of two seconds) to evaluate potential quench reactions. Glass analyses and potentiometric analyses of quenched aqueous fluids from the rapid-quench experiments are statistically comparable to those in the traditional cold-seal runs. Thus, quench reactions do not appear to affect the charge. Capsules were removed from the vessels, cleaned, examined microscopically, and weighed to determine if the capsules remained sealed during the experiment. Only capsules that exhibited mechanical integrity and no mass change (±3 mg)were processed for analysis. Petrographic examination of all experimental run products indicated that the phase assemblage consisted of glass (i.e., quenched melt), magnetite, aqueous fluid, and the quartz chip.

2.4. Demonstration of Equilibrium

We did not perform reversal experiments as part of the current study. Thus, we must rely on other data to demonstrate that the fluids trapped in quartz microfractures represent equilibrated solute loads (Simon et al., 2003a). Here we combine the results of two series of experiments that allow us to evaluate the method of synthetic fluid inclusion entrapment in prefractured quartz crystals as a means of quantifying accurately both the major- and trace-element solute load of coexisting two-phase immiscible fluids in the experimental charge. One set of experiments trapped Au-saturated NaCl-KCl-$FeCl_2$-HCl-H_2O vapor and brine fluids inside self-healing quartz microfractures as fluid inclusions at the *PVTX* run conditions. The quenched experimental fluid not trapped inside quartz was recovered from the capsule after quenching to ambient conditions. A second set of experiments trapped brine in vesicles of quenched melt (Frank et al., 2002). The solute loads of quenched aqueous vapor, from experiment setup 1, and brine trapped in vesicles, from experiment setup 2, represent fluid samples that were in equilibrium with the charge until experiment termination and are compared with fluids trapped as inclusions in quartz before quench. Fluid inclusions trapped in quartz microfractures were analyzed by LA-ICPMS. The quenched fluid from runs of setup 1 was analyzed by atomic absorption spectrophotometry (AAS). The solute load of brine in vesicles was determined by instrumental neutron activation analysis (INAA) using mass balance constraints. The major-element (i.e., Fe, K, Na) solute loads of synthetic vapor inclusions and quenched fluids overlap at the 2σ uncertainty level. Gold concentrations in the synthetic brine inclusions trapped in quartz microfractures overlap the gold concentrations of brine trapped in melt vesicles at the 2σ uncertainty level. These data suggest that quartz microfractures heal on a slow enough timescale to allow the entrapment of equilibrated synthetic vapor and brine fluid inclusions at *PVTX* conditions relevant to Earths' upper crust. Our results demonstrate the effectiveness of using prefractured quartz to trap coexisting two-phase fluids in a single experimental charge.

2.5. Analytical Procedures

2.5.1. Potentiometric analyses of quenched fluids to infer HCl concentrations

Recovered capsules were placed in dry ice to cool the quenched vapor inside the capsule. After several minutes of cooling, the top end of the capsule (i.e., end of capsule elevated furthest from the horizontal plane on which the experimental apparatus assembly rests) was pierced with a stainless steel hypodermic syringe. Cooling the capsule prevented strong egress and loss of fluid due to overpressure inside the capsule. The quenched aqueous solution was removed using the hypodermic syringe and transferred to a weighed volumetric flask. Recovered aqueous solutions were weighed and diluted for potentiometric analyses (pH). Recovered solutions were not filtered before analysis. The HCl concentration of the quenched experimental fluids was inferred by measuring fluid pH using a Beckman φ40 pH meter equipped with an AccupHast electrode. To quantify properly the activity vs. concentration function for hydrogen ion in the quenched solutions we prepared pH standards with reagent grade HCl to define a pH range that overlapped the expected pH of the quenched solutions, and we added reagent grade NaCl and KCl in proportions corresponding to the concentrations of these salts in the quenched experimental solutions. Expected concentrations were determined by analyzing the quenched aqueous fluid for sodium and potassium, using AAS, from one experiment at each pressure. This procedure minimizes the matrix effect error on the measured pH values. The determined M_{H^+} (25°C) in the quenched fluid is assumed to represent the hydrogen ion concentration that was present as associated HCl in the experimental fluid as HCl completely dissociates during quench (Tagirov et al., 1997). Although this assumption ignores the possibility of subsolidus reactions that can affect the M_{H^+} we minimized possible quench effects by analyzing recovered charges within one to two hours of quench. Additionally, the three rapid-quench reconnaissance experiments yielded fluids with statistically similar pH values. Thus, quench problems were avoided and the use of quench pH (25°C) to infer HCl is valid. Table 3 lists the concentration of HCl in experimental solutions.

It should be noted that the potentiometrically determined hydrogen concentrations represent the hydrogen in the quenched aqueous fluid, consisting of both vapor and brine quenched from run conditions. The calculated mass proportion of vapor:brine in all experiments was determined by using the lever rule, the data for salinity of the starting aqueous solution, and the measured wt% NaCl eq. values of vapor and brine fluid inclusions. Recall that the proportion of vapor: brine is >95:1 by weight at all experimental conditions; we feel that at the low total HCl in the quenched magmatic fluids the contribution of HCl to the quenched aqueous mixture is insignificant owing to the expected partitioning of HCl in vapor relative to brine (Williams et al., 1997). We note that using the lever rule in the model NaCl-H_2O system to determine mass proportions of vapor and brine in a more complex NaCl-KCl-$FeCl_2$-HCl-H_2O system may introduce a component of error into these conclusions. However, the absolute change in salinities of coexisting vapor and brine along the solvus in the more complex system does not appear to change more than one weight percent relative to the model NaCl-H_2O system. For example, Bodnar et al. (1985) report that the wt% NaCl values for vapor and brine are 6 and 51 at 800°C and 130 MPa in the model NaCl-H_2O system. The current study indicates that the wt% NaCl eq. values for vapor and brine, respectively, range from 4.9 to 5.3 and 50 to 53 at 800°C and 130 MPa in the more complex NaCl-KCl-$FeCl_2$-HCl-H_2O system. Thus, while the solvus is enlarged slightly with the addition of KCl, $FeCl_2$, and HCl, the magnitude of this salinity change does not significantly affect the calculated mass ratios of vapor and brine determined by applying the lever rule to the NaCl-H_2O system.

2.5.2. Analyses of experimental glasses

Quantitative characterization of Si, Al, Na, K, Fe, and Cl silicate glass (i.e., quenched haplogranite melt) was performed by wavelength dispersive spectrometry (WDS) using a JEOL JXA 8900 electron microprobe. Samples were prepared for analysis by coating them with a ~0.03 μm carbon film using standard thermal evaporation techniques. Operating conditions for glass analyses were 15 keV accelerating potential, 5 nA beam current, and 15 μm beam size with minimum counting times of twenty seconds (sum of peak and background). Analyses of glass at multiple locations indicated that the silicate glasses are homogeneous with respect to major elements and chlorine. As pointed out by Morgan and London (1996) and Acosta-Vigil et al. (2003), sodium migration and concomitant aluminum and silicon burn-in during the analysis of hydrous aluminosilicate glasses can cause significant analytical bias. We performed multiple analyses to determine if these phenomena occurred and found no systematic sodium migration in glasses with variable sodium and water concentrations. Yellowstone haplogranite (National Museum of Natural History, NMNH 72854 VG568) was used to standardize Si, Al, Na, and K. Kakanui hornblende (United States National Museum, USNM 143956) was used to standardize Fe. Scapolite (Meionite, Brazil, USNM R6600-1) was used to standardize Cl.

The gold concentration of silicate glasses was quantified using LA-ICPMS. We analyzed spots that were petrographically devoid of fluid inclusions and magnetite crystals (e.g., Simon et al., 2003b) and also integrated the host glass signal intervals from analyses of magnetite crystals trapped within quenched melt. A National Institute of Standards and Technology (NIST) standard reference material, NBS-610, was used as the reference silicate glass. The transient signal for each analysis was integrated, and the concentration of silicon, determined from EPMA, was used to quantify all other oxide components of the glass.

2.5.3. Fluid inclusion microthermometry

Recovered chips of Brazilian quartz were agitated ultrasonically in doubly deionized and distilled H_2O for 30 min to remove surficial contaminants. The quartz chips were placed in Crystal Bond, sectioned longitudinally into wafers (~500 μm thick) and then doubly polished for petrographic examination, microthermometry, and LA-ICPMS analysis. Petrographic examination of polished quartz sections indicate that vapor and brine were trapped as fluid inclusions as well as inclusions containing a mixture of both. Vapor inclusions contain only liquid plus vapor bubble whereas brine inclusions contain liquid, vapor

Table 3. LA-ICPMS data for synthetic fluid inclusions of coexisting vapor and brine fluid inclusions.

P (MPa)	# of runs	Type of Inclusions Analyzed	Number of Inclusions Analyzed	Initial[1] wt% NaCl eq.	Final[2] wt% NaCl eq.	HCl[3] μg/g (±2σ)	pH[4]	Na μg/g (±2σ)	K μg/g (±2σ)	Fe μg/g (±2σ)	Au μg/g (±2σ)
110	3	Vapor	17	2.5	2.1–2.4	970 ± 110	1.57	5500 ± 840	5800 ± 800	3100 ± 740	5 ± 2
		Brine	12		56–58	ND[5]	ND[5]	140000 ± 8000	150000 ± 16000	64000 ± 6000	29 ± 4
130	4	Vapor	13	5	4.9–5.3	1000 ± 260	1.56	9500 ± 2200	14000 ± 2000	10000 ± 2600	4 ± 1
		Brine	6		50–53	ND[5]	ND[5]	110000 ± 10000	130000 ± 20000	72000 ± 20000	28 ± 4
140	2	Vapor	8	10	8.8–9.3	1100 ± 230	1.52	17000 ± 6900	27000 ± 6000	20000 ± 2000	28 ± 8
		Brine	6		42–44	ND[5]	ND[5]	82000 ± 6000	110000 ± 10000	73000 ± 18000	40 ± 10
145	3	Vapor	10	20	18.7–19.2	670 ± 90	1.73	32000 ± 6900	66000 ± 6000	41000 ± 2000	36 ± 11
		Brine	8		35–37	ND[5]	ND[5]	59000 ± 18000	120000 ± 40000	72000 ± 16000	50 ± 7

[1] Initial wt% NaCl eq indicates the salinity of the starting aqueous solution recast as wt% NaCl eq.
[2] Final salinities are the range of wt% NaCl eq values for synthetic vapor and brine fluid inclusions as determined by microthermometry.
[3] HCl concentrations inferred from potentiometrically determined hydrogen ion concentrations in quenched fluids.
[4] pH of the quenched aqueous mixture.
[5] ND = not determined.

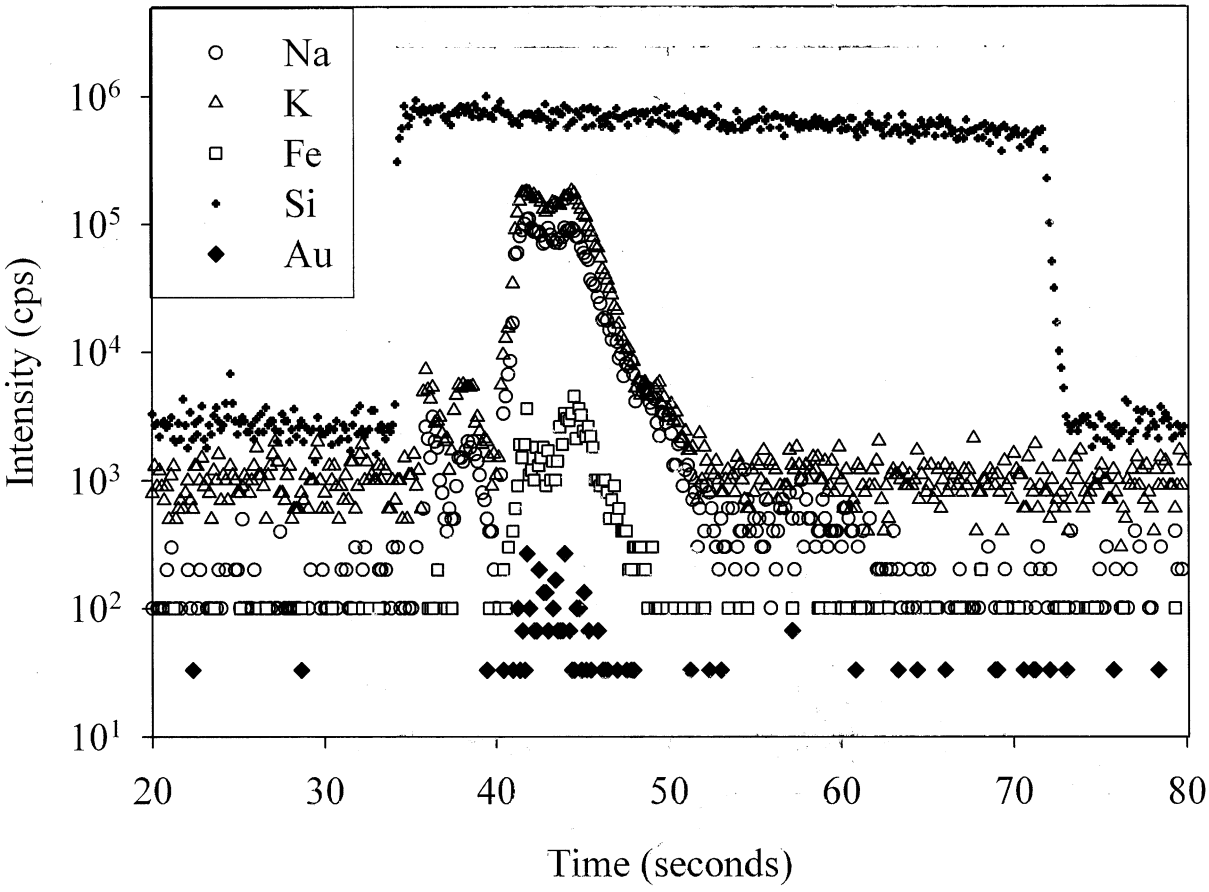

Fig. 2. LA-ICPMS transient signal of a vapor fluid inclusion (~23 μm across, ~20 μm deep, 19 wt% NaCl eq.) hosted within quartz. A 30 μm beam diameter was used to ablate the entire inclusion. Ablation of quartz began at ~35 s and the fluid inclusion was liberated from ~40 to 53 s. The first twenty seconds of gas background are not shown to emphasize the fluid inclusion and host signal.

bubble, and multiple mineral phases. At least one visible salt crystal is visible in all brine inclusions, and magnetite, inferred from crystal morphology and the ability to move the crystal with a strong magnet, is visible in some. Salinities of vapor and brine inclusions were determined by freezing-point depression (i.e., Tm_{ice}) and final dissolution of halite (i.e., Td_{NaCl}), respectively (Bodnar and Vityk, 1994). Microthermometric measurements were performed using a USGS-type gas-flow heating-freezing stage (Fluid, Inc.) The thermocouple was placed directly on the sample and served to hold the sample stationary during measurements and to reduce the uncertainty in temperature measurements owing to minimal distance of the thermocouple tip and the fluid inclusion assemblage. Apparent salinities for magmatic vapors and brines expressed as NaCl equivalent (wt% NaCl eq.) were calculated using the equations of Bodnar and Vityk (1994) and are reported in Table 3. The wt% NaCl eq. values presented are the range for all fluid inclusions analyzed at a given pressure. Only fluid inclusions that trapped pure vapor and pure brine (i.e., no fluid inclusions containing a mixture of vapor + brine) and gave freezing and heating temperatures consistent with Bodnar and Vityk (1994) were chosen for analysis by LA-ICPMS.

2.5.4. *LA-ICPMS analyses of synthetic fluid inclusions*

The solute concentrations of synthetic individual vapor and brine inclusions were quantified by LA-ICPMS using an energy-homogenized (Microlas) pulsed 193-nm ArF Excimer laser (Compex 110i, Lamda Physik) that enables controlled ablation (Günther et al., 1997, 1998; Heinrich et al., 2003). ICPMS machine settings were similar to those reported in Pettke et al. (2004). Laser ablation was performed in a 1 cm^3 ablation chamber and monitored with a video camera that permitted constant observation of the sample surface during ablation. The diameter of the laser beam was set slightly larger than the maximum dimension of each fluid inclusion such that the entire inclusion was ablated together with a minimal volume of surrounding matrix quartz.

A representative LA-ICPMS transient signal of a vapor inclusion (~23 μm diameter; 19 wt% NaCl eq.) from a depth of ~20 μm is shown in Figure 2. The signal consists of gas background (0–34 s and 73–100 s), quartz (34–40 and 49–73 s), and quartz plus vapor fluid inclusion (40–49 s). The transient signal for each analysis was integrated, and element ratios (e.g., Au:Na) were quantified using an NIST standard reference material NBS-610 silicate glass. The ability of silicate glass standards to quantify solute loads of fluid inclusions has been demonstrated by Günther et al. (1998) as well as our own reconnaissance experiments briefly summarized in section 2.4. Element ratios determined by LA-ICPMS were transformed into absolute element concentrations using sodium as the internal standard (Heinrich et al., 2003). Absolute concentrations of sodium in each fluid inclusion were determined by correcting the wt% NaCl eq., determined by microthermometry for the presence of KCl and $FeCl_2$ via the equation

$$NaCl_{true} = NaCl_{equiv} - 0.5 \times \sum X^{n+}Cl_n \quad (1)$$

which treats all major cations in the fluid inclusion as chloride salts (Heinrich et al., 2003). Note that element ratios, and thus partition coefficients, are independent of this assumption.

3. RESULTS

3.1. Gold Concentrations in Vapor, Brine and Melt

3.1.1. The gold content of magmatic vapor

The concentrations of gold and major elements in synthetic vapor fluid inclusions as well as the inferred HCl and pH of quenched experimental aqueous fluids are presented in Table 3. The concentration of gold ($\pm 2\sigma$) decreased by an order of magnitude as pressure was decreased from 145 to 110 MPa while maintaining 800°C. Figure 3a shows a marked increase in the Au-carrying capacity of mildly acidic magmatic vapor as pressure increases above 130 MPa at 800°C and $f_{O_2} = NNO$. The data indicate that between 110 ($C^v_{Au} = 5$ μg/g) and 130 MPa ($C^v_{Au} = 4$ μg/g), there is no change in the gold-carrying capacity of gold-saturated magmatic vapor. Even with the relatively high uncertainty associated with data at 140 and 145 MPa, the gold concentration increases by an order of magnitude as pressure increases to 140 MPa (C^v_{Au} μg/g).

3.1.2. The gold content of magmatic brine

The concentrations of gold in synthetic brine fluid inclusions coexisting with vapor also are presented in Table 3. Gold concentrations in brines increase by nearly a factor of two as pressure was increased from 110 to 145 MPa while maintaining 800°C (Fig. 3b). Similar to the data presented above for vapor fluid inclusions, the data for brine make evident that pressure plays a role in the gold-carrying capacity of magmatic brine. There is essentially no change in the Au-carrying capacity of brine between 110 ($C^b_{Au} = 29$ μg/g) and 130 MPa ($C^b_{Au} = 28$ μg/g). However, as pressure increases from 130 to 145 MPa, the gold content of brine increases by almost 60%, to $C^b_{Au} = 50$ μg/g. Note that with increasing pressure, the salinity of the brine coexisting with vapor decreases along the solvus. Therefore, the increase in gold solubility with pressure cannot be related directly to brine chlorinity—other parameters are required to account for this observation.

3.1.3. The gold content of haplogranite melt

EPMA data for the experimental glasses (Table 4) indicate that all experimental melts were mildly peralkaline (i.e., ASI = 0.86 to 0.95; ASI calculated as the molar ratio $Al_2O_3/(Na_2O + K_2O)$). These data indicate that the starting synthetic glass experiences an increase in its abundance of sodium and potassium owing to mass transfer between the aqueous fluids and the melt. LA-ICPMS results show that the solubility of gold in haplogranite melt is on the order of 250–500 ng/g at pressures between 100 and 145 MPa (Table 5). These gold solubility data are lower than those determined in previous studies. Jugo et al. (1999) reported gold solubility in *S*-bearing Au-saturated haplogranite melt at 850°C and 100 MPa to be on the order of 2 to 4 μg/g, albeit at higher HCl concentrations than in our experiments. Frank et al. (2002) reported a Au solubility at 800°C and 100 MPa in *S*-free Au-saturated haplogranite melt on the order of 1 μg/g. Gold concentrations in these earlier studies were determined by secondary ion mass spectrometry (SIMS) and/or instrumental neutron activation analysis (INAA). As discussed by Frank et al. (2002), it is possible that the quenched silicate glasses produced in their experiments contained submicroscopic gold nuggets or regions of increased gold concentration within the glass that formed during quenching. Frank et al. (2002) discussed the nugget effect, with specific reference to INAA and SIMS, and concluded that the best estimate of gold solubility in haplogranite melt was on the order of 1 μg/g. It should also be noted that the experiments of Jugo et al. (1999) included fluids that contained significantly higher HCl concentrations that increase the potential of generating heterogeneities during quenching. In light of the subtle differences between the experimental configurations of all these studies, we think that the LA-ICPMS determination of gold concentration on the order of 500 ng/g in haplogranite glass provides currently the best estimate for gold solubility in *S*-free haplogranite melt.

4. GOLD SOLUBILITY IN MAGMATIC FLUIDS

4.1. Gold Speciation

Our experiments do not allow us to evaluate directly the gold species present in either vapor or brine. However, using data from other studies we can suggest hypotheses regarding the gold speciation in our experimental vapors. The critical pressure at 800°C in the NaCl-H_2O binary system is ~160 MPa (Anderko and Pitzer, 1993). With decreasing pressure, the salinity, hence chloride content, of brine-saturated vapor continuously decreases (Fig. 1), and the consequence of decreasing chloride ligands may be a decrease in the concentration of any chloride-complexed metal (Simon et al., 2004). In contrast, the salinity of the brine increases with decreasing pressure. The only study of the speciation of gold at the temperature and pressure conditions attending the early evolution of a devolatilizing gold-bearing magma suggests that gold is present in acidic (i.e., HCl > 11,000 ppm) magmatic brine as the neutral gold-chloride complex, $AuCl_2H^O$ (Frank et al., 2002). These authors performed experiments to elucidate the effect that C^b_{HCl} has on the gold-carrying capacity of vapor-undersaturated brine at 100 MPa, 800°C, and $f_{O_2} = NNO$. Their data yield two distinct trends in C^b_{Au} vs. C^b_{HCl} space. At $C^b_{HCl} > 11 \times 10^3$ μg/g the data fit a regression line whose slope is equal to approximately two, suggesting that the complex of gold in the brine has a gold:chloride ratio of 1:2 at the *PVTX* conditions of their experiments. This ratio is consistent with gold being present as $AuCl_2H^O$ (AuCl *x* HCl) in the brine when $C^b_{HCl} > 11 \times 10^3$ μg/g. Their data suggest no relationship between C^b_{Au} and C^b_{HCl} when $C^b_{HCl} < 11 \times 10^3$ μg/g (0.3 molal HCl). Based on these data, Frank et al. (2002) postulate that a gold-hydroxide complex, $AuOH^O$, dominates gold speciation in high-temperature low-HCl brines (i.e., brines with $C^b_{HCl} < 11 \times 10^3$ μg/g). They proposed that the relationship between chlorido- and hydroxide-complexed gold in magmatic brine is controlled by the equilibrium

$$AuOH^b + 2HCl^b = AuCl_2H^b + H_2O \quad (2)$$

Frank et al. (2002), following the model of Williams et al. (1997), report that the concentration of HCl in natural brines exsolved from felsic melt, with an aluminum saturation index (ASI) = 1.01, is ~11×10^3 μg/g. Increasing peraluminosity will drive the HCl concentration of the brine to values as high

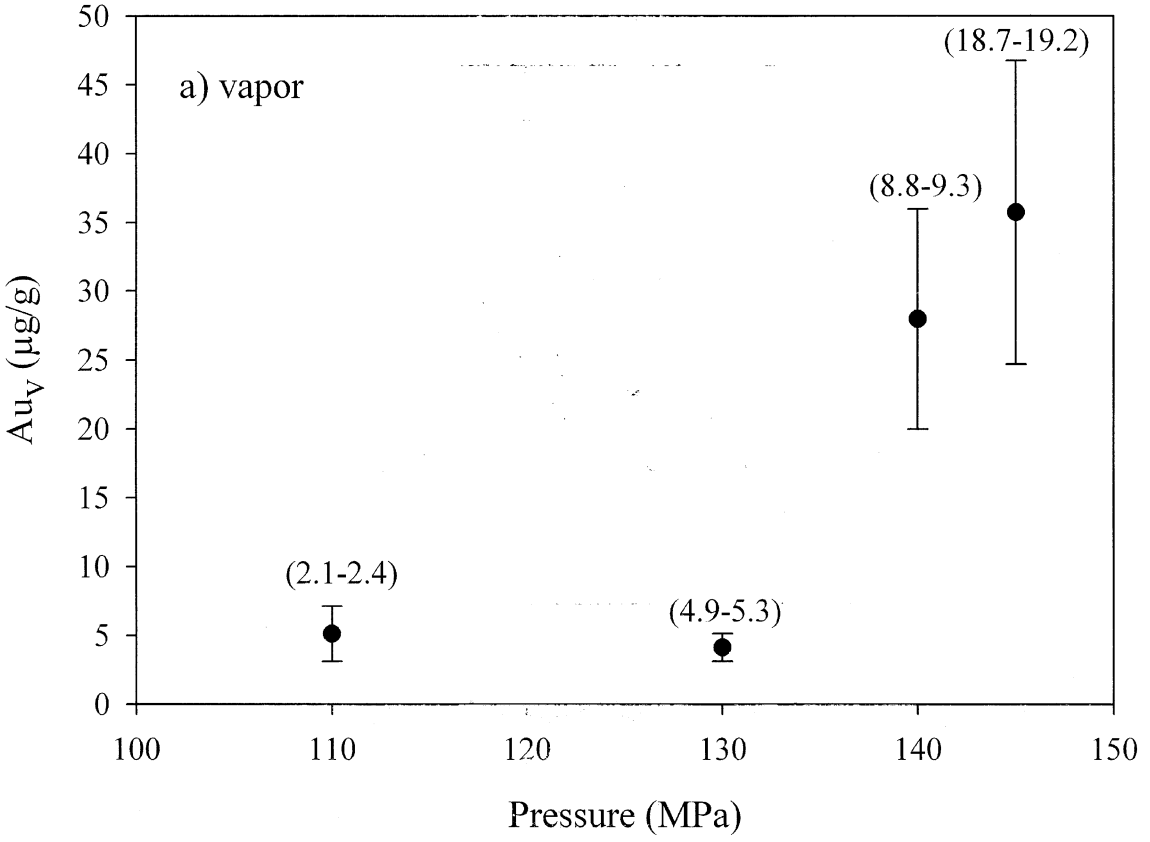

Fig. 3. The concentration of gold in (a) vapor and (b) brine as a function of pressure. Experiments performed at 800°C and f_{O_2} = *NNO*. The wt% NaCl eq. of vapor fluid inclusions increased from ~2 to ~19 as pressure was increased from 110 to 145 MPa at constant temperature. The wt% NaCl eq. of brine fluid inclusions decreased from ~57 to ~36 as pressure was increased from 110 to 145 MPa at constant temperature. Numbers in parentheses are the range of measured salinities at each pressure expressed as wt% NaCl eq.

Table 4. EPMA analyses of major elements and chlorine in the run product glasses. All data expressed as wt% ($\pm 2\sigma$).

P (MPa)	SiO_2	K_2O	Na_2O	FeO	Al_2O_3	Cl	Total	ASI
110	73.06 ± 1.33	4.88 ± 0.29	4.43 ± 0.65	1.40 ± 0.37	10.92 ± 0.77	0.20 ± 0.04	94.89	0.87
130	72.65 ± 1.30	5.21 ± 0.28	4.30 ± 0.46	1.09 ± 0.30	10.97 ± 0.99	0.22 ± 0.05	94.44	0.86
140	73.54 ± 2.07	5.16 ± 0.35	3.77 ± 0.53	1.03 ± 0.29	10.43 ± 0.99	0.21 ± 0.06	94.14	0.89
145	72.72 ± 1.54	5.21 ± 0.26	3.34 ± 0.42	1.07 ± 0.28	9.78 ± 0.82	0.20 ± 0.03	92.32	0.88

Each datum represents the average of a minimum of ten spot analyses in different areas of a given experimental glass. ASI was calculated as the molar ratio $Al_2O_3/(Na_2O + K_2O)$. The calculated values of ASI indicate that all experimental melts were peralkaline. Uncertainties are presented as twice the standard deviation from the mean ($\pm 2\sigma$) for the replicate measurements of each glass.

as 37×10^3 μg/g (Frank et al., 2002). These considerations suggest that the gold species $AuOH^O$ may be dominant in HCl-poor magmatic fluids, of variable salinity, exsolved from peralkaline to peraluminous melts. The chloride to hydroxide shift could also be effected at lower temperature (i.e., <550°C) by a combination of Eqn. 2 and the equilibrium

$$3KAlSi_3O_8^{kfs} + 2HCl^{fl} = KAl_2Si_3AlO_{10}(OH)_2^{ms} + 6SiO_2^{qtz} + 2KCl^{fl} \quad (3)$$

that describes the neutralization of HCl-bearing fluids due to reaction with country rock through which the fluid migrates.

We did not determine the acidity of brines from our experiments. The HCl concentrations and pH (25°C) reported in Table 3 were determined from the quenched aqueous mixture. We infer these HCl and pH values to represent those of the experimental vapor because of the strong fractionation of HCl into vapor relative to brine at high temperatures and the small mass fraction of brine in the quenched aqueous mixture. If Eqn. 2 is taken to be applicable to magmatic vapors, then our data, to a first approximation, appear to be consistent with $AuOH^O$ as the dominant gold-bearing species in low-density aqueous magmatic fluids at the *PVTX* conditions of our experiments. However, data in the current study do not allow us to test directly this hypothesis and, therefore, we must rely on inferences based on our data combined with those from other studies.

To our knowledge there are no extant experimental data demonstrating the existence of $AuOH^O$ in either magmatic vapor or brine at the *PT* conditions of the current study. Frank et al. (2002) inferred the existence of $AuOH^O$ in brine based on the decoupling of gold and chloride concentrations in experimental brines at low HCl concentrations. However, there are extant experimental data that demonstrate the existence of $AuOH^O$ in low-chloride (0–2000 μg/g) aqueous solutions at temperatures lower than those in the present study (Zotov et al., 1985, 1991, 1994; Bailey et al., 1997; Gammons et al., 1997; Stefánsson and Seward, 2003). Bailey et al. (1997) used in situ XAFS to determine gold speciation in mildly acidic aqueous solutions with variable chloride concentrations at temperatures lower than 300°C. They reported that gold-hydroxide complexes replace gold-chloro complexes with increasing temperature up to 175°C from $[AuCl_4^-]$ at pH = 4, but that as the fluid becomes more neutral the chloride ligands were replaced by OH^- ligands and the dominant gold species was $AuOH^O$.

Stefánsson and Seward (2003a) report that gold solubility in chloride- and sulfur-free aqueous vapor varies from 1.2×10^{-8} to 2.0×10^{-6} molal (i.e., 2 to 400 pg/g) at temperatures and pressures ranging from 300°C to 600°C and 50 to 150 MPa, respectively. Their experimental solutions contained no complexing ligands apart from the hydroxide species, OH^-. Their study conclusively demonstrates that gold speciation in weakly acidic, pH ≈ 4, to alkaline hydrothermal solutions is dominated by $AuOH^O$. Equilibrium constants, $K_{s,1}$, for the dissolution of gold as $AuOH^O$ were presented as

$$K_{s,1} = \frac{(C_{Au}^v)(f_{H_2})^{0.5}}{(a_{Au})(a_{H_2O})} \quad (4)$$

where $K_{s,1}$ is the equilibrium constant for gold dissolution as $AuOH^O$, C_{Au}^v is the concentration of gold in vapor, f_{H_2} is hydrogen fugacity, a_{Au} is the activity of gold, and a_{H_2O} is the activity of water. The activities of gold and water were taken as unity, given saturation with respect to pure gold and low ionic strength of the recovered experimental solutions. The determined values for $K_{s,1}$ increase from 300°C to 400°C and are then independent of both pressure and temperature between 50 and 150 MPa and 400°C and 600°C. Log $K_{s,1}$ varies from a high of −7.66 ± 0.08 at 600°C and 100 MPa to a low of −7.50 ± 0.11 at 500°C and 150 MPa. These values of $K_{s,1}$ indicate that the concentration of gold as $AuOH^O$ is insensitive to changes in both temperature and pressure between 50 and 150 MPa and 400°C and 600°C.

Here we assume explicitly that the increase in temperature from 600°C to 800°C does not significantly affect the values of $K_{s,1}$. This assumption allows us to evaluate the possibility that $AuOH^O$ is the dominant gold species present in the experimental vapors of the current study. This assumption is based on the near-complete absence of pressure and temperature dependence of gold solubility as determined by Stefánsson and Seward (2003a). Our vapors contain chloride, ranging from 0.36 to 3.24 molal, as pressure increases from

Table 5. Partition coefficients ($\pm 2\sigma$) for gold between coexisting vapor, brine and melt at 800°C and variable pressures.

P (MPa)	$D_{Au}^{v/m}$	$D_{Au}^{b/m}$	$D_{Au}^{v/b}$
110	10 ± 4	58 ± 23	0.17 ± 0.04
130	8 ± 5	56 ± 23	0.14 ± 0.07
140	56 ± 32	80 ± 38	0.80 ± 0.26
145	72 ± 31	100 ± 41	0.72 ± 0.12

110 to 145 MPa, whereas the experiments reported by Stefánsson and Seward (2003a) were chloride free. Thus, we simply use their data to calculate the expected concentration of gold as $AuOH^o$ at our experimental conditions. This provides a reasonable baseline upon which to evaluate whether additional gold species may be present in the higher temperature vapors of the current study. Rearranging the equilibrium constant for gold dissolution as $AuOH^o$ (Eqn. 4) to solve for gold concentration at our experimental conditions yields

$$C^v_{Au} = \frac{(K_{s,1})(X^v_{H_2O})}{(f_{H_2})^{0.5}} \quad (5)$$

Note that this formalism does not contain a_{Au} owing to the gold-saturated nature of our experiments. We assumed Raoultian behavior (i.e., $a^v_{H_2O} = X^v_{H_2O}$) for water and used the mole fraction of water. Note that Stefánsson and Seward (2003a) assumed an $a^v_{H_2O}$ equal to unity; however, using $X^v_{H_2O}$ accounts for the increased salinity of our experiments. This calculation yields a gold solubility as $AuOH^o$ on the order of 10×10^{-9} molal (0.002 μg/g) at 800°C and 110 to 145 MPa. This calculated solubility of gold is significantly lower than those determined in the current study. If the extrapolation of $K_{s,1}$ yields accurate gold concentration data at our experimental *PT* conditions, these calculations suggest that one or more additional gold species is present in our experimental vapors. Thus, the potential existence of chloridogold(I) species must be evaluated.

A second study by Stefánsson and Seward (2003b) reports the solubility of chloridogold(I) complexes in aqueous solutions from 50 to 180 MPa and 300°C to 600°C. They studied experimentally the solubility of gold and evaluated statistically, using nonlinear least-squares fits, the stability of the gold species $HAuCl^+$, $H_2AuCl_2(aq)$, $AuCl(aq)$, $AuCl_2^-$, and $AuClOH^-$. Their data suggest that the gold species $AuCl_2^-$ is the most stable chloridogold(I) species at their experimental *PVTX* conditions, with the equilibrium written as

$$Au(s) + 2Cl^- + H^+ = AuCl_2^-(aq) + 0.5H_2(g) \quad (6)$$

Stefánsson and Seward (2003b) calculate and report the stability of $AuCl_2^-(aq)$ relative to $AuOH^o$ across a pH range from 0 to 9 and a chlorinity ranging from 0.001 to 1.0 molal. They report that a model with the gold(I) chloride species, $AuCl_2^-(aq)$, and the gold hydroxide species, $AuOH^o$, is the most statistically favored at the conditions of their experiments. At 600°C, 150 MPa, and $m_{Cl} = 1.0$, their data demonstrate that $AuCl_2^-$ dominates gold speciation from pH = 0 to 4; that is, 100% percent of the gold in aqueous vapor is present as $AuCl_2^-$. With increasing pH above 4, the stability of $AuOH^o$ becomes important. At a pH of ~5.5 gold speciation is divided almost equally between $AuCl_2^-$ and $AuOH^o$, and by a pH of 7 the proportion of gold present as $AuOH^o$ increases to ~90%. Thus, the data sets of Stefánsson and Seward (2003a, b) indicate that $AuCl_2^-$ and $AuOH^o$ dominate gold speciation in aqueous solutions at low and high pH, respectively, across a pressure and temperature range of 50 to 180 MPa and 300°C to 600°C. Furthermore, their data suggest the existence of chloridogold(I) species in our experimental vapors. We can not use their data to evaluate directly gold speciation in brines in the current study owing to differences in chloride concentration between the experimental studies.

The concentrations of gold, at gold saturation, in aqueous solutions at 600°C reported by Stefánsson and Seward (2003b) are 2.1×10^{-6} (4.1×10^{-4}) and 6.5×10^{-6} (1.2×10^{-3}) at 100 and 150 MPa and a constant pH of 9×10^{-3}. Note that these pH values are three orders of magnitude lower than those in the current study (Table 3); however, we can use these data to evaluate the change in gold concentration as a possible chloridogold(I) species as temperature increases from 600°C to 800°C. Based on the quantity of gold hypothesized to be present as $AuOH^o$, the quantity of chloridogold(I) is on the order of 99% of the gold present in vapors produced in the current experimental study. This is in agreement with the model of Stefánsson and Seward (2003b), which demonstrates that the a non gold-hydroxide species dominates in vapors with pH < 4. An important point to note is that at the temperature of the current study the stability of neutral species is favored relative to charged species such as $AuCl_2^-$. Thus, we do not use their values for the equilibrium constant for gold dissolution as $AuCl_2^-$ (Eqn. 6) to calculate expected concentrations of $AuCl_2^-$ at our experimental conditions. Stefánsson and Seward (2003b) conclude that the neutral *AuCl* is not present in aqueous vapor at 600°C. Thus, we do not expect this complex to dominate the gold species in aqueous vapor and brine at higher temperatures. However, we can hypothesize the existence of a neutral chloridogold(I) species at the *PVTX,* pH (25°C), and hydrogen fugacity conditions of the current study and evaluate the correlation between gold and chloride concentrations in our experimental vapors as a function of pressure to test this hypothesis.

We did not vary the chloride concentration of experiments at a given pressure; however, the chloride concentration of vapors in the current study did change as a function of pressure from 110 to 145 MPa. Thus, here we examine the relationship between gold and chloride concentrations as a function of increasing chlorinity to evaluate the hypothesis that chloridogold(I) species are present in our experimental vapors. Figure 4 shows the change in gold concentration as a function of the chloride concentration of vapors produced in this study. The gold concentration remains statistically unchanged with increasing chlorinity from 0.36 to 0.87 molal as pressure increases from 110 to 130 MPa (Table 3). This suggests tentatively that if gold is present as a chloridogold(I) species, there is no increase in the solubility of gold owing to increasing chloride concentration with increasing pressure from 110 to 130 MPa. Note that these results do not refute the existence of a gold-chloride species. There is a fivefold increase in the gold concentration as the chlorinity of the vapor phase increases with increasing pressure above 130 MPa. The average slope between 130 and 145 MPa is 1.6 and this suggests a gold:chloride ratio of approximately two (Fig. 4). Gold is monovalent at the conditions of our experiments and, thus, these data are consistent with the presence of $HAuCl_2$ as written in Eqn. 2 above. Although Frank et al. (2002) postulate that $AuOH^o$ is the dominant gold species in aqueous brines containing $C^b_{Hcl} < 11 \times 10^3$ μg/g, data in the current study coupled with data from Stefánsson and Seward (2003a, b) are not consistent with $AuOH^o$ being the dominant gold-species in our experi-

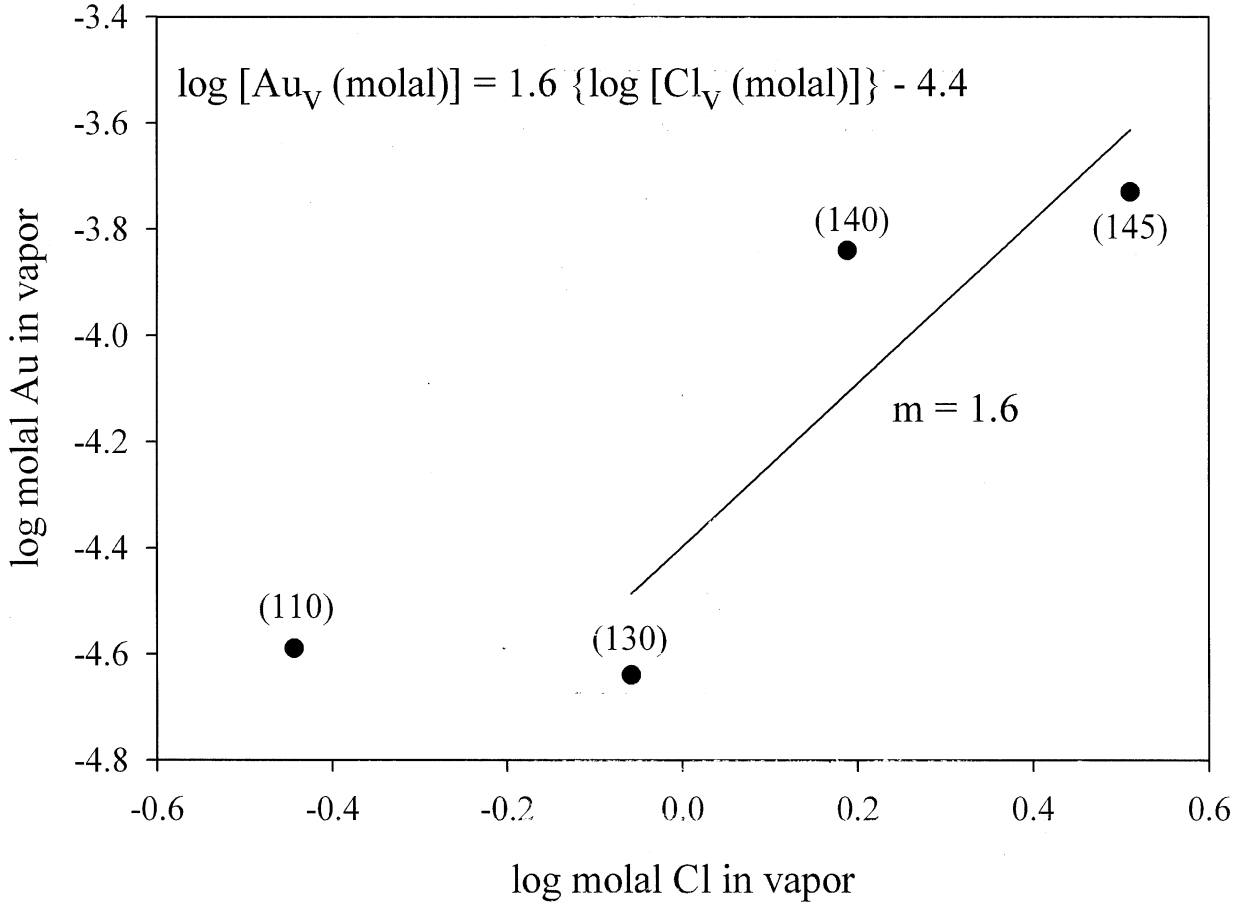

Fig. 4. Experimentally determined molality of gold vs. molality of chlorine in synthetic vapor fluid inclusions. Numbers in parentheses indicate the pressure of each datum.

mental aqueous vapors. Note that the presence of $HAuCl_2$ is inferred from the concentration dependence of gold vs. chloride with increasing pressure that yields a slope of approximately two. We stress that more experimental data are needed to quantify accurately the equilibria that control gold solubility in acidic to near-neutral aqueous vapors at the *PVTX* conditions of the current study. Additionally, experiments in a vapor-undersaturated brine-melt system are required to quantitatively evaluate gold speciation in hypersaline liquids. In this paper we simply provide a framework upon which future studies will build.

4.2. Gold Partitioning Between Vapor and Brine

4.2.1. Sulfur-free magmatic fluids

Calculated mass partition coefficients for gold between coexisting vapor, brine and haplogranite melt are reported in Table 5. These brine/melt and vapor/melt partition coefficients underscore that partitioning of Au into a fluid (brine or vapor) from a *S*-free haplogranite melt increases with increasing pressure. The partition coefficient for gold between vapor and brine decreases from 0.7 to 0.2 as pressure decreases from 145 MPa to 110 MPa. The value of D_{Au}^{vb} is constant, within the uncertainty of our data set, from 145 MPa to 140 MPa and from 130 to 110 MPa. Figure 5 shows that vapor fractionation increases strongly with increasing pressure. These partition coefficients have important implications for the role that the boiling process has on gold transport in the magmatic-hydrothermal environment.

4.2.2. Sulfur-bearing magmatic fluids

Over the past decade there have been an increasing number of data from natural vapor-brine boiling assemblages indicating that gold can sometimes partition preferentially into magmatic vapor relative to coexisting brine (e.g., Heinrich et al., 1999). The physicochemical mechanism to explain the selective mass transfer of gold to the vapor phase during boiling remains unidentified. The preferential partitioning of gold into the vapor phase during the boiling process has been postulated to result from the strong affinity of metal-sulfur complexes for the vapor phase (Heinrich et al., 1999). However, unpublished data from Frank (2001) indicate that gold-sulfur complexes do not result in preferential mass transfer of gold into a vapor phase during boiling at a select set of *PVTX* conditions. Frank (2001) used LA-ICPMS to quantify the concentration of gold in coexisting sulfur-bearing synthetic vapor and brine fluid inclusions produced in a haplogranite + vapor + brine + intermediate solid solution + pyrrhotite + bornite + gold metal assemblage at

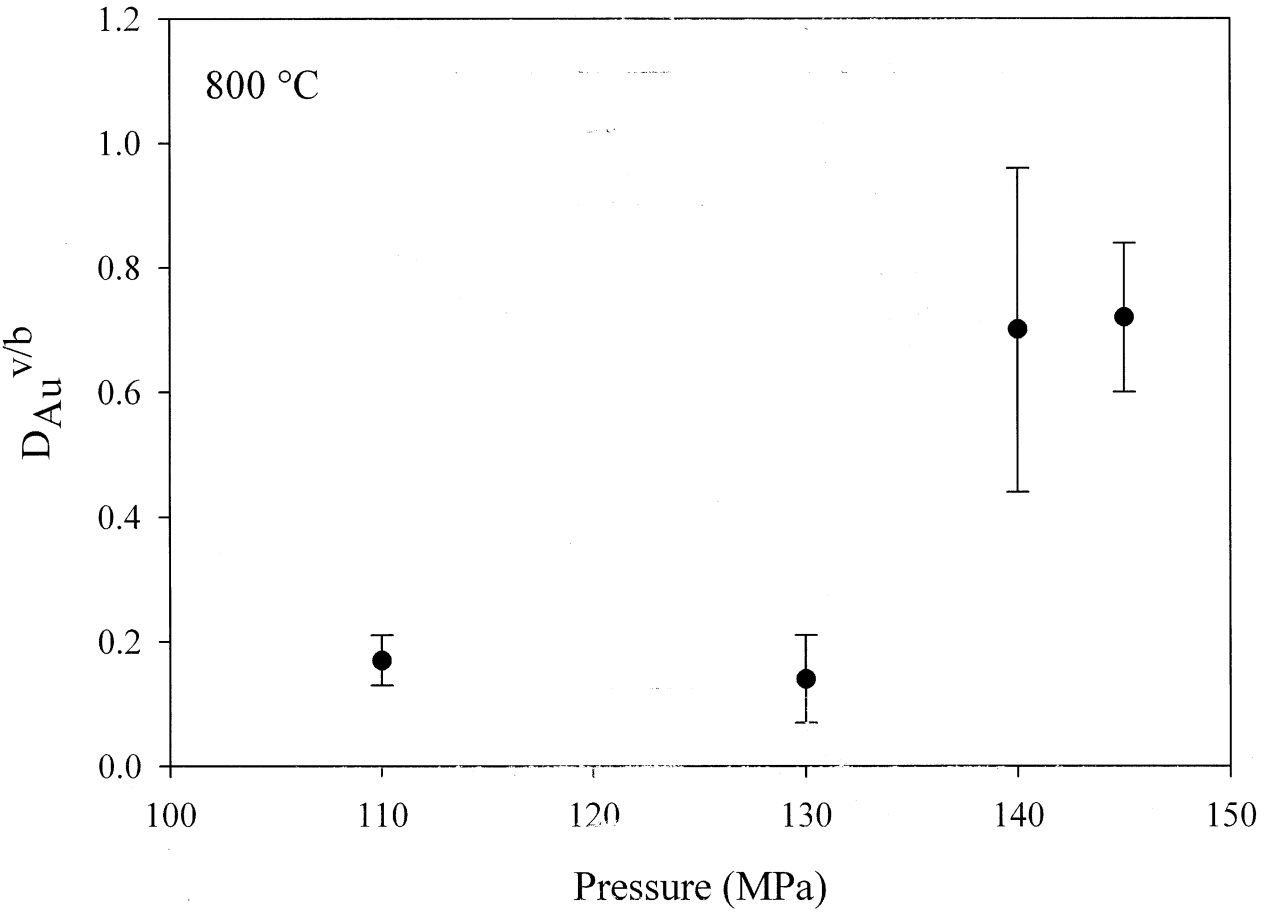

Fig. 5. The experimentally determined partition coefficients for gold between coexisting vapor and brine as a function of pressure at 800°C and oxygen fugacity buffered at NNO.

800°C, 100 MPa, and oxygen fugacity buffered at NNO. The concentration of HCl in the magmatic fluids in his experiments did not exceed 1000 μg/g, and thus these data are directly comparable to those in the present study. The concentration of gold in brine range from 48 to 240 μg/g and in vapor from 16 to 24 μg/g, resulting in vapor/brine partition coefficients, $D_{Au}^{v/b}$, of less than one. The sulfur fugacity in his experiments was calculated following Barton (1973) and reported as $f_{S_2} = -3.8$ at 800°C and 100 MPa. We calculated, using free energy data from Robie et al. (1979), that the H_2S/SO_2 ratio equals ~9 at the experimental conditions reported in Frank (2001). Frank (2001) does report an increase in gold solubility in sulfur-bearing brines relative to sulfur-free brines and that this increased solubility may be a result of the gold-sulfur species $AuHS^o$. These experimental data agree with numerous data from natural vapor-brine boiling assemblages where the determined $D_{Au}^{v/b}$ is less than one (e.g., Ulrich and Heinrich, 2001). However, these experimental data do not shed light on the observed preferential partitioning of gold into vapor relative to brine in boiling assemblages from deposits such as Grasberg. It should be pointed out that these experimental data provide only a snapshot at a set of $P - T - f_{S_2} - f_{H_2S} - f_{O_2}$ conditions. Heinrich et al. (1999), citing the stability of Au(I)-bisulfide in reduced vapor (Benning and Seward, 1996) and the prevalence for vapor fractionation of copper in reduced Sn-W veins, suggest that preferential partitioning of metals into vapor may be enhanced in reduced systems with even higher sulfur fugacities than those reported by Frank (2001).

Recent experimental work by Nagaseki and Hayashi (2004) suggest that the hypothesis of Heinrich et al. (1999) may be correct. Nagaseki and Hayashi (2004) report data from experiments that trapped synthetic, coexisting, gold-bearing vapor and brine fluid inclusions in quartz microfractures. Experiments were performed at conditions between 400°C and 600°C from 20 to 50 MPa. A synchrotron x-ray fluorescence microprobe was used to quantify the solute loads of the synthetic vapor and brine fluid inclusions. Their data indicate that gold partitions preferentially into vapor relative to coexisting brine at high f_{S_1} within the temperature and pressure range of their study. These data make clear that further experimental studies at higher temperature and pressure, at variable $f_{S_2} - f_{H_2S} - f_{O_2}$ conditions, are required to elucidate the physicochemical processes responsible for the observed tendency for preferential vapor fractionation of gold and other metals (e.g., As, Cu) in natural boiling magmatic fluids.

5. CONCLUSIONS

Data from this experimental study elucidate the partitioning behavior of gold as a function of pressure and chlorinity

between brine, vapor, and haplogranite melt. It is demonstrated that the gold-carrying potential of sulfur-free magmatic vapor and brine are roughly equivalent at pressures near the 800°C critical pressure, ~160 MPa, in the NaCl-KCl-$FeCl_2$-HCl-H_2O system when the concentration of HCl of the aqueous phase is low (i.e., HCl $\leq$ 1100 μg/g). These data illustrate that the ability of coexisting magmatic vapor and brine to scavenge and transport gold from a felsic melt is a direct function of the converging chloride concentrations in the coexisting fluids with increasing pressure along the solvus in the gold-saturated NaCl-KCl-$FeCl_2$-HCl-H_2O system. We infer gold speciation in experimental vapors to be dominated by the complex $HAuCl_2$. The strong positive correlation between pressure, chlorinity of the aqueous phases, and gold concentrations in aqueous vapor and brine demonstrates that, for a given set of conditions, magmatic devolatilization occurring at higher pressures favors a larger quantity of gold being transported from magma into the superjacent environment. We presented limited discussion of sulfur's effect on the partitioning behavior of gold between melt, vapor, and brine, and we stress that much more experimental research is required if we are to constrain fully the physicochemical behavior of gold in magmatic fluids at variable *PVTX* conditions relevant to magmatic conditions.

Acknowledgments—This work was partially supported by National Science Foundation (EAR 9909576 (PAC and PMP); EAR 0125805 (PAC and PMP); EAR 9810244 (PMP)), a Cosmos Club Foundation Student Research Grant, and University of Maryland Graduate School Ilene H. Nagel Research Grant to ACS. We thank Artas Migdisov, D. C. "Bear" McPhail, Associate Editor Liane Benning, and two anonymous reviewers for their constructive and helpful comments. ACS also thanks Terry Seward for informal communication regarding gold speciation. ACS thanks Bruce Marsh for allowing time to write this manuscript and for providing a new framework with which to view processes. ACS also thanks Abigail and James for their insatiable love of performances and baseball which provided much needed and enjoyable diversions. The Fluid and Ore Deposits Group at ETH acknowledges continued support for LA-ICPMS analytical development by the Swiss National Science Foundation.

Associate editor: Liane Benning

REFERENCES

Acosta-Vigil A., London D., Morgan G. B., and Dewers T. A. VI (2003) Solubility of excess alumina in hydrous granitic melts in equilibrium with peraluminous minerals at 700–800 C and 200 MPa and applications of the aluminum saturation index. *Contrib. Mineral. Petr.* **146,** 100–119.

Anderko A. and Pitzer K. S. (1993) Equation-of-state representation of phase equilibria and volumetric properties of the system NaCl-H_2O above 573 K. *Geochim. Cosmochim. Acta* **57,** 1657–1680.

Audétat A. and Pettke T. (2003) The magmatic-hydrothermal evolution of two barren granites: A melt and fluid inclusion study of the Rito del Medio and Canada Pinabete plutons in northern New Mexico (USA). *Geochim. Cosmochim. Acta* **67,** 97–121.

Audétat A., Günther D., and Heinrich C. A. (1998) Formation of a magmatic hydrothermal ore deposit; insights in with LA-ICP-MS analysis of fluid inclusions. *Science* **279,** 2091–2094.

Audétat A., Günther D., and Heinrich C. A. (2000) Magmatic-hydrothermal evolution in a fractionating granite: A microchemical study of the Sn-W-F-mineralized Mole Granite (Australia). *Geochim Cosmochim Acta* **64,** 3373–3393.

Bailey, E. H., Schofield, P. F., and Mosselmans, J. F. W. (1997) Gold complexation by chloride bearing fluids—an XAFS study. In *Seventh Annu. V.M. Goldschmidt Conference*, Lunar and Planetary Institute, Houston, LPI Contribution No. 2264.

Barton, P. B., (1973) Solid solutions in the system Cu-Fe-S: Part I: The Cu-S and Cu-Fe-S joins. *Econ Geol* **68,** 455–465.

Belonoshko A. B., Shi P. F., and Saxena S. K. (1992) A FORTRAN-77 program for calculation of Gibbs free energy and volume of C-H-O-S-N-Ar mixtures. *Comp. Geosci.* **18,** 1267–1269.

Benning L. G. and Seward T. M. (1996) Hydrosulfide complexing of gold(I) in hydrothermal solutions from 150 to 500°C and 500 to 1500 bars. *Geochim. Cosmochim. Acta* **60,** 1849–1872.

Bodnar R. J. (1995) Fluid inclusion evidence for a magmatic source for metals in porphyry copper deposits. In *Mineralogical Association of Canada Short Course, Vol. 23, Magmas, Fluids and Ore Deposits* (ed. J. F. H. Thompson), pp. 139–152. Mineralogical Association of Canada.

Bodnar R. J. and Vityk, M. O (1994) Interpretation of microthermometric data for H_2O NaCl fluid inclusions. In *Fluid Inclusions in Minerals, Methods and Applications*, (eds. B. De Vivo and M. L. Frezzotti), pp. 117–130. Virginia Polytechnic Institute.

Bodnar R. J., Burnham C. W., and Sterner S. M. (1985) Synthetic fluid inclusions in natural quartz. III. Determination of phase equilibrium properties in the system H_2O-NaCl to 1000C and 1500 bars. *Geochim. Cosmochim. Acta* **49,** 1861–1873.

Burnham C. W. (1979) Magmas and hydrothermal fluids. In *Geochemistry of Hydrothermal Ore Deposits* (ed. H. L. Barnes), pp. 71–136. Wiley, New York.

Candela P. A. (2004) Ores in the Earth's crust. In *The Crust* (ed. R. L. Rudnick), *Treatise on Geochemistry* (eds. H. D. Holland and K. K. Turekian), Vol. 3. Oxford, Elsevier.

Candela P. A. and Holland H. D. (1984) The partitioning of copper and molybdenum between melts and aqueous fluids. *Geochim. Cosmochim. Acta* **48,** 373–380.

Charles R. W. and Vidale R. (1982) Temperature calibration of a new rapid quench vessel. *Am. Mineral.* **67,** 175–179.

Chou I. C. (1987a) Phase relations in the system NaCl-KCl-H_2O: III, Solubilities of halite in vapor-saturated liquids above 445 degrees C and redetermination of phase equilibrium properties in the system NaCl- H_2O to 1000 degrees C and 1500 bars Geochim. *Cosmochim. Acta* **51,** 1965–1975.

Chou I. C. (1987b) Oxygen buffer hydrogen sensor techniques at elevated pressures and temperatures. In *Hydrothermal Experimental Techniques* (eds: G. C. Ulmer and H. L. Barnes) pp 61–99.

Drummond S. E. and Ohmoto H. (1985) Chemical evolution and mineral deposition in boiling hydrothermal systems. *Econ. Geol.* **80,** 126–147.

Dutrizac J. E. (1976) Reactions in cubanite and chalcopyrite. *Can. Mineral.* **14,** 172–181.

Emmons W. H. (1927) Relations of disseminated copper ores in porphyry to igneous intrusions. *Am. Inst. Mining Metall. Eng. Trans.* **75,** 797–809.

Fournier R. O. (1987) Conceptual models of brine evolution in magmatic-hydrothermal systems. *U. S. Geol. Surv. Prof. Pap.* **1350,** 1487–1506.

Frank M. R. (2001) An experimental investigation of ore metals in silicate melt-volatile phase systems. Ph.D. dissertation, Univ. of Maryland.

Frank M. R., Candela P. A., and Piccoli P. M. (1998) K-feldspar-muscovite-andalusite-quartz brine phase equilibria: An experimental study at 25–60 MPa and 400–550°C. *Geochim. Cosmochim. Acta* **62,** 3717–3727.

Frank M. R., Candela P. A., Piccoli P. M., and Glascock M. D. (2002) Gold solubility, speciation and partitioning as a function of HCl in the brine-silicate melt-metallic gold system at 800°C and 100 MPa. *Geochim. Cosmochim. Acta* **66,** 3719–3732.

Gammons C. H. and Williams-Jones A. E. (1997) Chemical mobility of gold in the porphyry epithermal environment. *Econ. Geol.* **92,** 45–59.

Gammons C. H., Yu Y., and Williams-Jones A. E. (1997) The disproportionation of gold(I) chloride complexes at 25 to 200°C. *Geochim. Cosmochim. Acta* **61,** 1971–1983.

Günther D., Frischknecht R., Heinrich C. A., and Kahlert H. J. (1997) Capabilities of an argon fluoride 193 nm excimer laser ablation

inductively coupled plasma mass spectrometry microanalysis of geological materials. *J. Anal. Atom. Spec.* **12,** 939–944.

Günther D., Audétat A., Frischknecht A., and Heinrich C. A. (1998) Quantitative analysis of major, minor and trace elements in fluid inclusions using laser ablation-inductively coupled plasma mass spectrometry. *J. Anal. Atom. Spec.* **13,** 263–270.

Halter W. E., Pettke T., and Heinrich C. A. (2002) The origin of Cu/Au ratios in porphyry type ore deposits. *Science* **296,** 1844–1846.

Hedenquist J. W. and Lowenstern J. B. (1994) The role of magmas in the formation of hydrothermal ore deposits. *Nature* **370,** 519–527.

Hedenquist, J. W., Arribas, A., Jr., Reynolds, T. J (1998) Evolution of an intrusion centered hydrothermal system; Far Southeast-Lepanto porphyry and epithermal Cu-Au deposits, Philippines. *Econ. Geol.* **93,** 373–404.

Heinrich C. A., Ryan C. G., Mernagh T. P., and Eadington P. J. (1992) Segregation of ore metals between magmatic brine and vapor. *Econ. Geol.* **87,** 1566–1583.

Heinrich C. A., Günther D., Audétat A., Ulrich T., and Frischknecht R. (1999) Metal fractionation between magmatic brine and vapor, determined by microanalysis of fluid inclusions. *Geology* **27,** 755–758.

Heinrich C. A., Pettke T., Halter W. E., Aigner-Torres M., Audétat A., Günther D., Hattendorf D., Bleiner D., Guillong M., and Horn I. (2003) Quantitative multi-element analysis of minerals, fluid and melt inclusions by Laser-Ablation Inductively-Coupled-Plasma Mass Spectrometry. *Geochim. Cosmochim. Acta* **67,** 3473–3497.

Henley R. W. and McNabb A. (1978) Magmatic vapor plumes and ground-water interaction in porphyry copper emplacement. *Econ. Geol.* **73,** 1–20.

Huebner J. S. and Sato M. S. (1970) The oxygen fugacity-temperature relationships of manganese oxide and nickel oxide buffers. *Am. Mineral.* **55,** 934–938.

Jugo P. J., Candela P. A., and Piccoli P. M. (1999) Linearly independent conditions of chemical equilibrium for the partitioning of ore metals in melt-crystal-volatile phase systems: Applications to mineral exploration. Second International Symposium on Granites and Associated Mineralizations, Salvador, Brazil. *Lithos* **46,** 573–589.

Lang J. R., Stanley C. R., Thompson J. F. H., and Dunne K. P. E. (1995) Na-K-Ca magmatic hydrothermal alteration in alkalic porphyry Cu-Au deposits, British Columbia. *Mineral. Assoc. Can. Short Course Ser.* **23,** 339–366.

Loucks R. R. and Mavrogenes J. A. (1999) Gold solubility in supercritical hydrothermal brines measured in synthetic fluid inclusions. *Science* **284,** 2159–2163.

Lowenstern J. B. (2001), Carbon dioxide in magmas and implications for hydrothermal systems, *Mineral. Dep.* **36,** 490–502.

Marschik R. and Fontboté L. (2001) The Candelaria–Punta del Cobre Iron Oxide Cu-Au(-Zn-Ag) deposits, Chile. *Econ. Geol.* **96,** 1799–1826.

Morgan G. B. VI and London D. (1996) Optimizing the electron microprobe analysis of hydrous alkali aluminosilicate glasses. *Am. Mineral.* **81,** 1176–1185.

Nagaseki H. and Hayashi K. (2004) Synthetic fluid inclusions in boiling hydrothermal solutions: Experiment in porphyry environments. Japanese-Swiss Seminar: "Spatial and temporal relationships between deep magmatic, porphyry and epithermal environments and significance for ore formation processes," Tsukuba and Kogoshima, Japan, March 8–14, 2004.

Pettke T., Halter W. E., Webster J. D., Aigner-Torres M., and Heinrich C. A. (2004) Accurate quantification of melt inclusion chemistry by LA-ICPMS: A comparison with EMP and SIMS and advantages and possible limitations of these methods. *Lithos* **78,** 333–361.

Piccoli P. M., Candela P. A., and Williams T. J. (1999) Constraints on estimating HCl and Cl in the magmatic volatile phase in granites and granite-related ore systems: A potential tool for the estimation of high- and low-Cl systems. Second International Symposium on Granites and Associated Mineralizations; Salvador, Brazil. *Lithos* **46,** 573–589.

Requia K., Stein H., Fontboté, L., and Chiaradia M. (2003) Re-Os and Pb-Pb geochronology of the Archean Salobo iron oxide-copper-gold deposit, Carajás mineral province, northern Brazil. *Mineral. Dep.*, **38,** 727–738.

Richards J. P., McCulloch M. T., Chappell B. W., and Kerrich R. (1991) Sources of metal in the Porgera gold deposit, Papua, New Guinea: Evidence from alteration, isotope and noble metal geochemistry. *Geochim. Cosmochim. Acta* **55,** 565–580.

Robie, R. A., Hemingway, B. S., and Fischer, J. R (1979) Thermodynamic properties of minerals and related substances at 298.15 K and 1 bar (10^5 Pascals) pressure and at higher temperatures. U. S. Geol. Surv. Bull., **1452,** 1–456.

Roedder, E (1984) Fluid inclusions, *Rev. Mineral.* **12,** 644 pp.

Shinohara H. and Hedenquist J. W. (1997) Constraints on magma degassing beneath the Far Southeast porphyry Cu-Au deposit, Philippines. *J. Petr.* **38,** 1741–1752.

Shinohara H. and Kazahaya K. (1995) Degassing processes related to magma-chamber crystallization. *Mineral. Assoc. Can. Short Course Ser.* **23,** 43–70.

Sillitoe R. H. (1979) Some thoughts on gold-rich porphyry copper deposits. *Mineral. Dep.* **14,** 161–174.

Sillitoe R. H (1989) Gold deposits in Western Pacific island arcs: the magmatic connection. In *The Geology of Gold Deposits: The Perspective in 1988*. Economic Geology Monograph, (eds. R. Keays,, R., and Ramsay, D.) Groves,, Economic Geology Monograph 6, pp. 274–291.

Sillitoe R. H (1993) Gold-rich porphyry copper deposits; geological model and exploration implications. In *Mineral Deposit Modeling*, Vol. 40, pp. 403–417. Geological Association of Canada.

Sillitoe R. H. (2000) Gold-rich porphyry deposits: descriptive and genetic models and their role in exploration and discovery, *Econ. Geol. Rev.*, **13,** 315–345.

Simon A. C., Frank M. R., Pettke T., Candela P. A., Heinrich C. A., and Piccoli P. M (2003a) Experiments using pre-fractured quartz to trap volatile phases: Can we believe the data? GSA 2003 Annual Meeting

Simon A. C., Pettke T., Candela P. A., Piccoli P. M., and Heinrich C. (2003b) Experimental determination of gold solubility in haplogranite melt and magnetite: constraints on magmatic gold budgets. *Am. Mineral.* **88,** 1644–1651.

Simon A. C., Pettke T., Candela P. A., Piccoli P. M., and Heinrich C. (2004) Magnetite solubility and iron transport in magmatic-hydrothermal environments, *Geochim. Cosmochim. Acta* **68,** 4905–4914.

Singer D. A. and Cox D. P. (1986) Grade and tonnage model of porphyry Cu-Au. *U. S. Geol. Survey Bull.* **1693,** 110–114.

Sourirajan S. and Kennedy G. C. (1962) The system $NaCl$-H_2O at elevated temperatures and pressures. *Am. J. Sci.* **260,** 115–141.

Stefánsson A. and Seward T. M. (2003a) The hydrolysis of gold(I) in aqueous solutions to 600°C and 1500 bar. *Geochim. Cosmochim. Acta* **67,** 1677–1688.

Stefánsson A. and Seward T. M (2003b) Stability of chloridogold(I) complexes in aqueous solutions from 300 to 600°C and from 500 to 1800 bar *Geochim. Cosmochim. Acta* **67,** 4559–4576.

Tagirov B. R., Zoo A. V., and Kingie N. N. (1997) Experimental study of dissociation of HCl from 350 to 500C and from 500 to 2500 bars: Thermodynamic properties of HCl, *Geochim. Cosmochim. Acta* **61,** 4267–4280.

Thompson J. F. H., Lang. J. R., Mortensen J. K., and Cassidy K. F. (1995) Cu-Au metallogeny of alkalic arc magmatism: Examples from the Mesozoic arc terranes of the northern Canadian Cordillera and comparison to the Tabar-Feni arc, PNG. Proc. Giant Ore Deposits–II Symposium, Queen's University, Kingston, Ontario, April 1995, 668–673.

Titley S. R. (1981) Geological and geotectonic setting of porphyry copper deposits in the southern Cordillera, *Ariz. Geol. Soc.* **14,** 79–97.

Ulrich T. and Heinrich C. A. (2001) Geology and alteration geochemistry of the porphyry Cu Au deposit at Bajo de la Alumbrera Argentina. *Econ. Geol.* **96,** 1719–1742.

Ulrich T., Günther D., and Heinrich C. A. (1999) Gold concentrations of magmatic brines and the metal budget of porphyry copper deposits. *Nature* **399,** 676–679.

Vila T. and Sillitoe R. H. (1991) Gold-rich porphyry systems in the Maricunga belt, northern Chile. *Econ. Geol.* **86,** 1238–1260.

Vlassopoulos D. and Wood S. A. 1990. Gold speciation in natural waters I: Solubility and hydrolysis reactions of gold in aqueous solution. *Geochim. Cosmochim. Acta* **54,** 3–12.

Williams T. J., Candela P. A., and Piccoli P. M. (1995) The partitioning of copper between silicate melts and two-phase aqueous fluids: An experimental investigation at kbar, 800°C and 0.5 kbar, 850°C. *Contrib. Mineral. Petr*. **121,** 388–399.

Williams T. J., Candela P. A., and Piccoli P. M. (1997) Hydrogen-alkali exchange between silicate melts and two-phase aqueous mixtures; an experimental investigation. *Contrib. Mineral. Petr*. **128,** 114–126.

Zotov A. V., Baranova N. N., Dar'yina T. G., and Bannykh L. M., and Kolotov V. P. (1985) The stability of $AuOH_{sol}$ in water at 300–500°C and 500–1500 atm. *Geochem. Int*. **1,** 105–110.

Zotov A. V., Baranova N. N., Dar'yina T. G., and Bannykh L. M. (1991) The solubility of gold in aqueous chloride fluids at 350–550°C and 500–1500 atm: Thermodynamic parameters of $AuCl_2^-$(aq) up to 750°C and 5000 atm. *Geochem. Int*. **28,** 63–71.

Zotov A. V., Kudrin A. V., Levin K. A., Shikina N. D. and Var'yash L. N. (1994) Experimental studies of the solubility and complexing of selected ore elements (Au, Ag, Cu, Mo, As, Sb, Hg) in aqueous solutions. In *Fluids in the Crust: Equilibrium and Transport Properties* (eds. K. I. Shmulovichet al.), pp. 95–137. Chapman & Hall, London.